Dissociation of Water at the MgO(100)−Water Interface: Comparison of Theory with Experiment

Michael A. Johnson, Eugene V. Stefanovich, and Thanh N. Truong*

Henry Eyring Center for Theoretical Chemistry, Department of Chemistry, University of Utah, Salt Lake City, Utah 84112

Jens Günster and D. W. Goodman*

Department of Chemistry, Texas A&M University, College Station, Texas 77843-3255

Received: September 16, 1998

Dissociative chemisorption of H_2O at the MgO(100)−water interface has been investigated both experimentally and theoretically. In particular, metastable impact electron spectroscopy (MIES) was used to image the density of occupied states on the MgO(100)/Mo(100) surface for various degrees of water exposure. After multilayer water desorption, spectral features typical of surface hydroxyls are present. To further study the possibility of dissociative chemisorption of water, a theoretical and computational method called CECILIA (combined embedded cluster at the interface with liquid approach) was used to calculate the geometry, energetics, and electronic density of states (DOS) for interfacial species. Consistent with experiment, our theoretical results predict that dissociative adsorption of H_2O at the MgO(100)−water interface is energetically more favorable than molecular adsorption. The stabilization of charged OH^- and H^+ interface adsorbates is due to polarization of the surrounding solvent.

1. Introduction

Ion sorption and chemical reactions at interfaces between metal oxides and water are central features in many natural and industrial processes. Examples include transportation of groundwater contaminants, electrode phenomena, corrosion, and dissolution. For geochemistry and atmospheric chemistry, surfaces of metal oxides are of particular interest as these compounds are major components of rocks, soils, and airborne dust particles. For many oxides it has been found that water molecules dissociate upon contact with the surface, forming various types of surface hydroxyl groups. It is also well-established that these hydroxyl groups play a decisive role in many chemical properties of oxide surfaces, including ion sorption, dissolution, and catalytic activity.[1]

MgO surfaces and their interactions with water have been extensively studied both theoretically and experimentally; however, the primary reason for our interest in the MgO−water system is the unsettled problem regarding chemical reactivity of the most stable MgO(100) surface toward water molecules. Many experimental[2−5] and theoretical[6−9] studies have found that water molecules do not dissociate upon adsorption on the MgO(100) crystal surface from vacuum. However, there are several experimental indications that water can dissociate at the MgO(100)−water interface. For example, the naturally occurring transformation of mineral periclase (MgO) to thermodynamically favored brucite ($Mg(OH)_2$) implies surface hydroxylation as an intermediate step. The commonly used argument to explain this transformation requires the involvement of low-coordinated surface sites[3,10−13] or high Miller index surface planes.[8,14−16] It is worthwhile to note that such defective structures are minority sites at the MgO surface. Moreover, this argument does not explain the independence of the initial rate of dissolution on the presence of defects and the formation of (100) facets upon immersion of MgO crystallites in water.[17] In addition, experimental studies show that the (100) surface dissolves in liquid water[18] and the rate of dissolution increases with increasing acidity.[19] It is also known that the presence of water can radically alter reaction mechanisms and kinetics at MgO surfaces.[20] All these facts suggest that hydroxylation of the MgO(100)−water interface is quite likely.

Structure and chemical properties of solid−liquid interfaces present a challenging test for both experiment and theory. In this article we apply novel experimental and theoretical techniques for studying dissociative chemisorption of a water molecule on the water-covered MgO(100) surface. For the detection of molecular water and its dissociation products adsorbed on the MgO surface, we employed metastable impact electron spectroscopy (MIES). This electron spectroscopic technique provides superior surface sensitivity and allows for direct imaging of the local density of occupied states on the surface (see ref 21 for a review). In addition, ab initio calculations were performed using the CECILIA model[22,23] (combined embedded cluster at the interface with liquid approach), which is the combination of an embedded cluster model[24,25] for representing interactions of the surface active site with the crystal lattice and the use of a dielectric continuum to model long-range polarization of the solvent. All computational conditions, i.e., cluster and embedding lattice size, pseudopotentials, basis sets, parameters of the solvation model, etc., are identical to those used in a recently published article[26] (referred to in this paper as article 1), so they will be repeated here only to the extent necessary for unity. In article 1 we reported on molecular H_2O interactions at the MgO(100)−vacuum and MgO(100)−water interfaces. We have shown excellent agree-

* Corresponding authors.

10.1021/jp983729r CCC: $18.00 © 1999 American Chemical Society
Published on Web 04/08/1999

ment between the energy profile for a single water molecule interacting with the MgO−water interface obtained using the CECILIA model and the density profile of water molecules predicted by molecular dynamics simulations using an ab initio derived potential force field.[27] Such consistency indicates that the CECILIA method can be a useful tool for the study of chemical interactions at solid−liquid interfaces.

The details and results of the experiments are presented in the next section, followed in section 3 by the results of our calculations. In section 4 we give a cumulative discussion of our results, and in section 5 we present the conclusions drawn from this work.

2. Experimental Section

2.1. Experimental Details. The experiments were carried out in an ultra-high-vacuum (UHV) system (base pressure $< 2 \times 10^{-10}$ Torr) which has been described in detail previously.[28] Briefly, the UHV system consists of two interconnected chambers: one for sample treatment, low-energy electron diffraction (LEED), and thermal programmed desorption (TPD) and the other for electron spectroscopy. In the latter there are facilities for X-ray photoelectron spectroscopy (XPS), Auger electron spectroscopy (AES), ultraviolet photoelectron spectroscopy (UPS), and metastable impact electron spectroscopy (MIES). In MIES, metastable excited helium atoms ($2^3S/2^1S$) are utilized to eject electrons from the substrate surface. In the case of insulating surfaces, the intensity of the ejected electrons versus their kinetic energy gives a direct image of the density of occupied states on the surface. Since the metastable helium atoms approach the surface with thermal kinetic energy (about 200 meV) this technique is nondestructive and highly surface-sensitive. For a more detailed introduction to MIES and its various applications in molecular and surface spectroscopy, see the recent review from Harada et al.[29] MIES and UPS spectra were measured simultaneously using a cold-cathode discharge source,[30,31] which provides both ultraviolet photons (HeI) and metastable He* ($E^* = 19.8/20.6$ eV). Metastable and photon contributions within the beam were separated by means of a time-of-flight method using a mechanical chopper. The energy denoted by E_F in the spectra of Figures 1 and 2 correspond to electrons emitted from the Fermi level of the Mo(100) substrate. In the following experimental spectra, all binding energies are referenced to E_F. Since the metallic Mo substrate and the analyzer are in electrical contact, the Fermi energy appears at a constant position.

MgO films were grown by depositing Mg in 1×10^{-6} Torr O_2 ambient on the Mo(100) surface at 550 K, followed by a 20-min annealing at 750 K in a 1×10^{-8} Torr O_2 background. The Mg source was made from a high-purity Mg ribbon wrapped around a tantalum filament. As shown in previous investigations, MgO films prepared under these conditions grow epitaxially on the Mo(100) substrate and their properties regarding the adsorption of water are very similar to those of MgO single crystals.[4,32,33] The quality of the MgO layers was checked by means of MIES, UPS, AES, and LEED. D_2O (CIL, 99.9%) was dosed after further purification via several freeze−pump−thaw cycles (vacuum distillation) by backfilling the UHV system. Since the water exposure in Langmuir (L, 1×10^{-6} Torr·s) was determined with a nitrogen calibrated ion gauge, the given exposures are only useful as relative values. The stability of the water partial pressure during dosage was confirmed with a mass spectrometer.

In the following presentation and discussion of our data, one monolayer (ML) of water is defined as the coverage which leads to the complete disappearance of the MgO substrate intensity in MIES. Provided that water adsorbs in a layer by layer fashion, this coverage would correspond, in accordance to ref 5, to a monomolecular layer with a density of one water molecule per surface MgO ion pair. A review of the literature, e.g., refs 3, 5, and 34, shows that the definition of one ML water on the MgO-(100) surface depends strongly on the applied method, and there exists no clear evidence for a layer by layer growth. However, loosely packed overstructures, such as (4×2) and (3×2), seem to cover the surface uniformly.

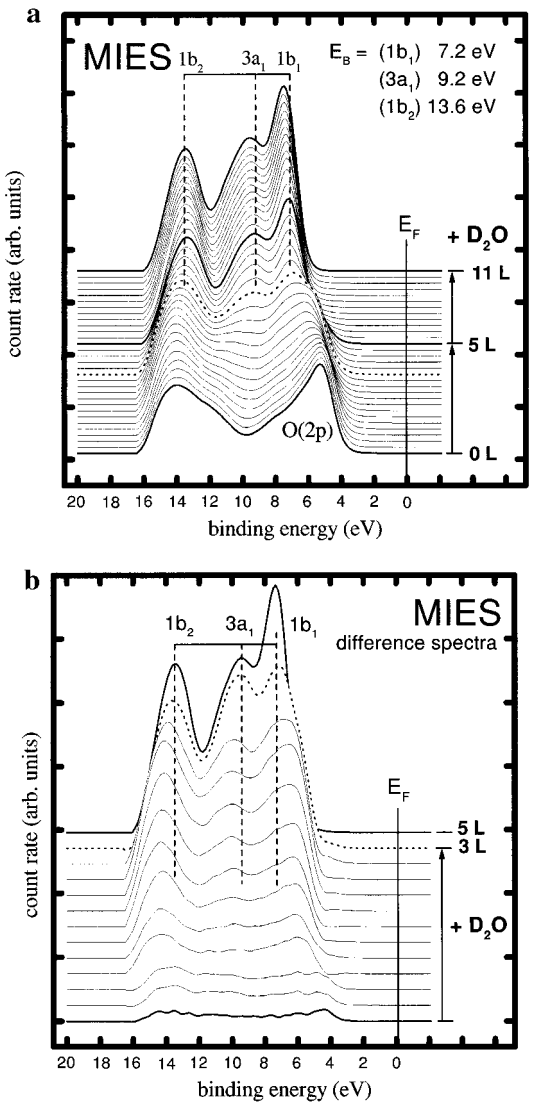

Figure 1. (a) MIES spectra from a 100 K MgO(100)/Mo(100) substrate as a function of D_2O exposure. The bottom spectrum shows the clean MgO(100) surface; the uppermost spectrum shows the surface covered by approximately 3 ML water. (b) Difference spectra obtained from the data presented in panel a.

2.2. Experimental Results. Since the electron spectroscopic data taken during exposure of water (D_2O) to the MgO-covered Mo(100) surface have been discussed in detail recently,[28] we will introduce this data only briefly in the present investigation. Figure la presents a sequence of MIES spectra collected during water exposure to the MgO/Mo(100) surface. Water was dosed (initially, 0.1 L/min, 0.3 L/spectrum) at a substrate temperature of 100 K. The spectrum of the clean MgO(100) surface (bottom spectrum in Figure la) agrees well with those reported previously.[35] The structure denoted by O(2p) corresponds to emission from the oxygen 2p valence band of the MgO(100) substrate.[35,36] Due to the insulating character of the clean MgO(100) surface,

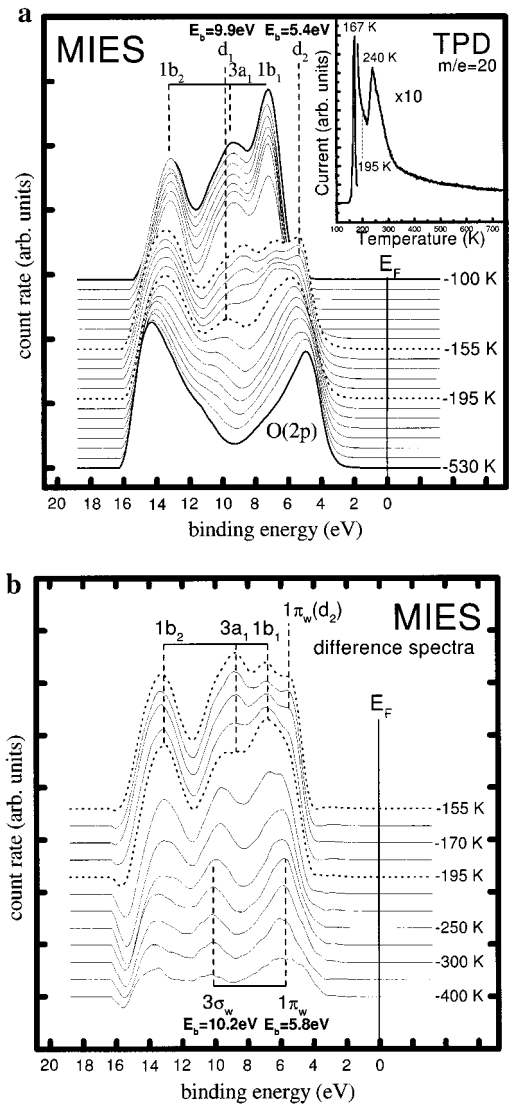

Figure 2. (a) MIES spectra taken from the surface prepared in Figure 1, i.e., MgO(100) covered by approximately 3 ML water, as a function of the anneal temperature. The inset presents a water desorption spectrum of the MgO(100) surface after dosage of 11 L water. (b) Difference spectra obtained from the data presented in panel a.

no intensity between E_F and 3.8 eV binding energy is apparent in the bottom spectrum. Thus no occupied states exist in resonance with the impinging He 2s electron, resulting in MIES spectra dominated by the Auger de-excitation process. This is an important prerequisite in order to gain direct information of the local density of states on the outermost substrate surface, i.e., to enabling a direct comparison between measurements and calculations. In the Auger de-excitation process, an electron from the substrate fills the 1s vacancy of the excited helium atom while the excess energy is transferred via an Auger process to the He 2s electron. Governed by the overlap between projectile and target orbitals, the probability of this process is proportional to the density of occupied states on the outermost substrate surface.[29] On the other hand, since the emitted electron originates from the helium atom, the density of empty states in the conduction band need not be taken into consideration for the interpretation of the MIES data.[21]

Starting from the bottom spectrum of the clean MgO surface in Figure 1a, there is a continuous build up of the water-induced features $1b_1$, $3a_1$, and $1b_2$ and an attenuation of the substrate intensity visible. Binding energies and molecular orbital assignments for the water-induced structures based on gas-phase photoelectron spectra[37,38] and penning ionization electron spectra (PIES)[39] are also given. In this context it is noteworthy that we found in a combined MIES and TPD study a water multilayer desorption feature in TPD far before the entire MgO surface had been covered by water molecules. This result suggests that initially, at water coverages up to about 0.5 ML, the water molecules adsorb in direct contact with the MgO surface: a wetting mode. However at coverages over 0.5 ML, already a significant amount of water adsorbs on top of the first layer: a mode of 3D island growth. It is unclear to what extent this island formation can be explained by a water bilayer formation.[2,34] Since there still exists considerable confusion concerning the growth mode in the initial stages of water adsorption on MgO(100), i.e., surface wetting versus clustering or the possibility of a water bilayer formation, a detailed discussion will be published elsewhere.[40] However, even at the present stage of our investigation we have to take into account that the first MIES spectrum in Figure 1a, which contains no contributions from the substrate (at 5 L), does not show water molecules in contact with the MgO surface only. Thus we have to focus our view on the subtle structural changes in the MIES spectra at very low water coverages in order to study a possible dissociation of water molecules in direct contact with the MgO(100) surface. For that reason, we present in Figure 1b difference spectra obtained from the data shown in Figure 1a. The curves in Figure 1b were obtained by subtracting the clean MgO spectrum, multiplied by a factor which takes the attenuated substrate intensity into account, from the data obtained after water dosage. Since the only features emerging from the difference spectra are the three water-induced bands $1b_1$, $3a_1$, and $1b_2$, the MIES data in Figure 1b support the model of nondissociative water adsorption on MgO(100) in a submonolayer coverage regime. It is important to point out that the difference spectra presented in Figure 1b do not provide the accuracy in terms of peak positions and intensities that are present in the original measurements of Figure 1a.

Figure 2a presents MIES spectra obtained from a water-covered MgO surface as a function of the substrate temperature. The uppermost spectrum shows the surface prepared in Figure 1a, i.e., MgO(100) covered by multilayer water at 100 K. The temperature threshold for the appearance of first significant changes in the MIES spectra is at about 155 K, which is in accordance with the onset of multilayer water desorption.[3] The inset presents a TPD spectrum obtained from a surface prepared under the same conditions as the one corresponding to the uppermost MIES spectrum in Figure 2a. The low-temperature desorption feature at 167 K corresponds to multilayer water desorption, the high-temperature feature at 240 K to the desorption of chemisorbed water in direct contact with the surface. In MIES, beside the water-induced structures, we find in the 155 K spectrum two new features: a shoulder in the $3a_1$ peak, denoted as d_1, and a prominent peak at 5.4-eV binding energy, denoted as d_2. At increasing substrate temperatures up to 195 K, the water-induced features together with d_1 and d_2 decrease in intensity. In accordance with the TPD data we attribute the MIES spectrum at 195 K to water molecules or their fragments in direct contact with the MgO surface. In order to have a more detailed look at the adsorbate-induced structures above 195 K, Figure 2b presents difference spectra obtained from the data in Figure 2a. Similar to Figure 1b, from the data obtained at the various substrate temperatures, we subtracted the clean MgO spectrum (bottom spectrum in Figure 2a) and multiplied by a factor which takes the attenuated substrate intensity into account. It is noteworthy that the enhanced

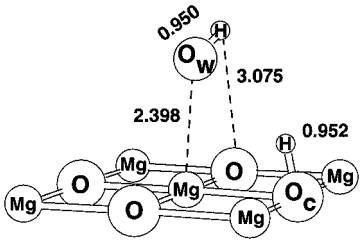

Figure 3. Optimized geometry for dissociated water at the MgO(100)−water interface ([MgO]H^+OH^-). Bond lengths are given in Å. This quantum cluster is embedded in the field of 247 additional pseudopotentials and point charges (not shown).

intensity at high binding energies visible in the bottom spectrum of Figure 2a is typically due to the applied heating current, which acts as an electromagnetic lens focusing preferably slow electrons from the substrate to the analyzer. This artificial intensity enhancement explains the appearance of the dip at the high-energy cutoff of the difference spectra in Figure 2b. Clearly visible in Figure 2b is the attenuation of d_2 between 155 and 170 K, while the intensity of the water-induced features remains almost constant. Over 195 K, the water structures vanish and a characteristic peak doublet, typical for surface hydroxyls,[41] appears, indicating a partial dissociation of water molecules. In this context, water dissociation at the water−MgO interface after multilayer water adsorption could be one explanation: Due to polarization in the water layers, charged hydroxyl species at the solid−liquid interface can be stabilized, and the dissociation of water becomes energetically favorable; this is discussed further in sections 3 and 4.

3. Theory

3.1. Computational Details. As mentioned in the Introduction, the computational model employed in this study is identical to that used in article 1 (ref 26), and that paper can be consulted for additional details.

We performed full geometry optimizations for molecular species H_2O, OH, OH^-, and H_3O^+ and the following surface species: [MgO]H_2O (physisorbed water on the [MgO] cluster), [MgO]H^+OH^- (dissociative chemisorption of water with OH^- adsorbed above the Mg site and H^+ adsorbed above a surface oxygen as in Figure 3), [MgO]OH^- (adsorbed hydroxide ion), [MgO]OH (adsorbed hydroxyl radical), and [MgO]H^+ (adsorbed proton). From the total energies of these optimized species we can calculate reaction energies and thus determine the plausibility of a hydroxylation process. The geometry optimizations utilized analytical energy gradients[42] and were performed using the Hartree−Fock approximation (HF). Electron correlation was accounted for in single-point second-order Møller−Plesset perturbation theory (MP2) calculations at the HF-optimized geometries. This correlation-corrected approach may result in about 1 kcal/mol difference in energy compared to full MP2 optimization.[43]

For all surface systems, except for the case of an adsorbed proton, the quantum cluster $[Mg_5O_4]^{2+}$ (for the sake of simplicity we refer to this cluster as [MgO]) was used to represent the substrate. This cluster forms a 3 × 3 square centered on a magnesium ion in the first surface layer. For a view of this cluster, see Figure 3 where this cluster is shown with a dissociatively adsorbed water molecule (see also Figure 1 in ref 26). For studying proton adsorption at a surface oxygen, we used a quantum cluster similar to that shown in Figure 3 with the exception that it is centered on an oxygen ion, giving the stoichiometry $[Mg_4O_5]^{2-}$; this provides a symmetric environment at the adsorption site. Ions in our cluster modeling the clean MgO(100) surface ([MgO]) were held fixed at rock salt lattice positions with a constant spacing of 2.1056 Å. For computational feasibility, ionic cores were approximated by effective core pseudopotentials (ECP).[44] The CEP-31G* basis set was used on the four oxygen ions (labeled "O" and "O_c" in Figure 3) nearest to the central Mg ion. The CEP-31G basis set was placed on the five Mg ions at the surface (labeled "Mg"). Additional lattice sites not shown in Figure 3 were modeled as either bare Mg pseudopotentials without basis sets, or point charges ($q_0 = \pm 2$), in order to represent the rest of the crystal. The entire system (cluster + point charges) consisted of four stacked 8 × 8 layers resulting in an 8 × 8 × 4 slab. This finite lattice has been shown to provide an accurate Madelung potential at the (100) rock salt crystal surface.[22,24] We used the standard valence CEP-31++G** basis set on adsorbed atoms (labeled O_w and H in Figure 3).

In the CECILIA approach, solvent effects are included by using the generalized conductor-like screening model (GCOSMO)[42,45−50] in which the liquid is represented as a dielectric continuum separated from the solute (in our case, crystal surface and adsorbate) by a sharp boundary. The boundary surfaces for CECILIA calculations were constructed using the GEPOL93 algorithm[51] as a set of interlocking spheres centered on nuclei. The atomic radii for these solvent cavity spheres have been optimized to yield hydration free energies for reactions in solution.[50] Therefore, energies reported in this article for reactions at the MgO−water interface include a free energy component from the liquid phase.

TABLE 1: Reaction Energies (kcal/mol) for Various Water-Related Species at the MgO(100) Surface and Aqueous Interface (values from other calculations in parentheses)

	reaction energy	
reaction	gas phase	liquid phase
(1) [MgO] + OH^- → [MgO]OH^-	−8.8	−8.0
(2) [MgO] + H^+ → [MgO]H^+	−242.3 (−164.9)[a]	−32.2[b]
(3) [MgO] + H_2O → [MgO]H^+OH^-(d)[c]	145.3	10.0
(4) [MgO] + OH → [MgO]OH	−10.4	
(5) [MgO] + H_2O → [MgO]H_2O	−14.2 (−17.3)[d]	+1.8
(6) [MgO] + H_2O → [MgO]H^+OH^-(nn)[e]	n/e[f]	−11.0

[a] From ref 53. [b] The reaction [MgO] + H_3O^+ → [MgO]H^+ + H_2O has been considered. [c] Distant proton/hydroxide ion pair. [d] From ref 27. [e] Nearest neighbor (nn) proton/hydroxide ion pair. [f] Does not physically exist.

3.2. Theoretical Results

Adsorption at the MgO−Vacuum Interface. In our previous theoretical study,[26] we found that water is physisorbed on the MgO(100) surface with a binding energy of 14.2 kcal/mol. In the present study, we investigated the possibility for dissociative chemisorption of water on this surface and found that it is not possible by a heterolytic nor a homolytic mechanism. Calculated total energies of the species listed at the beginning of section 3.1 can be used to estimate energetics for the adsorption reactions presented in Table 1. The energy gained by adsorption of OH^- (8.8 kcal/mol) and H^+ (242.3 kcal/mol) at the MgO−vacuum interface is not sufficient to overcome the heterolytic dissociation energy of water that we found to be 396.4 kcal/mol using the MP2//HF methodology. Note that our calculated dissociation energy is in good agreement with the experimental value of 390.5 kcal/mol,[52] indicating a sufficient amount of accuracy in the level of theory we have employed. In sum, the reaction energy of 145.3 kcal/mol (reaction 3 in Table 1)

required to hydroxylate the clean MgO(100) surface by adsorption of OH^- and H^+ at isolated surface sites is rather high. Regarding a homolytic dissociation mechanism, the MgO-(100)-H potential at the HF level was found by Pacchioni et al. to be repulsive.[53] We performed the MP2//ROHF calculation for the interaction of an OH radical with MgO(100), and this calculation yields a rather shallow minimum of 10.4 kcal/mol. Therefore, the interaction of neutral H and OH species with the MgO(100) surface cannot compensate for the energy of 119 kcal/mol[25] required to break the O−H water bond in a homolytic fashion. Thus, dissociation of water into two adsorbed radicals (H and OH) is not plausible either. From these energetic considerations and our attempts to locate a stable pair of neighboring surface OH^- and H^+ ions (or OH and H radicals), we suggest that molecular water adsorption at the MgO(100)−vacuum interface is more favorable than hydroxylation of the surface; this is in agreement with other experimental and theoretical studies.[9,15]

Adsorption at the MgO−Water Interface. Since hydration effects are most pronounced in the chemistry of charged species, we do not expect a solvent to significantly affect the adsorption behavior of neutral OH and H by providing an energy gain on the order of 100 kcal/mol that is required to stabilize the dissociative adsorption. Therefore, we conclude that the chemisorption of water with formation of OH and H radicals is not plausible at the water interface as well as on the clean oxide surface.

To calculate the energetics of proton adsorption at the oxide−solution interface, we need a good description of the hydrated proton. It is well known that a simple continuum model (a point charge in a dielectric cavity) does not provide an adequate description. However, H_3O^+ is a reasonable model for a hydrated proton.[54] Optimizing the geometry of H_3O^+ in solution we found that the reaction:

$$H^+(g) + H_2O(aq) \rightarrow H_3O^+(aq)$$

$$\Delta E^{MP2//HF} = -263.3 \text{ kcal/mol}$$

represents proton hydration energetics rather well in comparison to the mean value of −259.5 kcal/mol determined by five separate measurements.[55]

Our calculations suggest that dissociation of water into charged OH^- and H^+ at the MgO(100)−water interface is energetically favorable. Following a similar procedure as in the previous section, we can estimate the adsorption energy for a distant OH^-−H^+ pair at the MgO−water interface. Reaction 3 in Table 1 is endothermic by only 10.0 kcal/mol at the water interface; thus the electrostatic attraction between OH^- and H^+ can, in principle, make the dissociation of H_2O into OH^- and H^+ adsorbed on neighboring sites energetically feasible. In agreement with this estimate, in addition to molecular water adsorption being endothermic by 1.8 kcal/mol (reaction 5 in Table 1), we were able to find a minimum corresponding to the formation of two hydroxyl groups according to reaction 6 in Table 1. The geometry of this dissociated form of adsorbed water is shown in Figure 3. Here, O_wH^- is bound to the lattice Mg^{2+} ion, and the proton makes a strong bond with the lattice oxygen ion whereby its bond with oxygen from the water molecule is virtually broken (O−H distance is 2.21 Å). However, some residual attraction between OH^- and H^+ species remains, keeping the HOH angle at about 98.9°, close to the value found for an isolated water molecule. This minimum, with adsorption energy of 11.0 kcal/mol, corresponds to a total energy that is 21.0 kcal/mol lower than for a separated, adsorbed, OH^-−H^+ pair. Thus our calculations predict that OH^- and H^+ can exist at the MgO−water interface as a nearest neighbor pair, and their diffusion away from each other is unfavorable. Our sampling of the potential energy surface in regions corresponding to both separated and neighboring OH^- and H^+ ions, as well as for molecularly adsorbed water, leads us to believe that, within the accuracy of the CECILIA model, the configuration shown in Figure 3 is a global minimum.

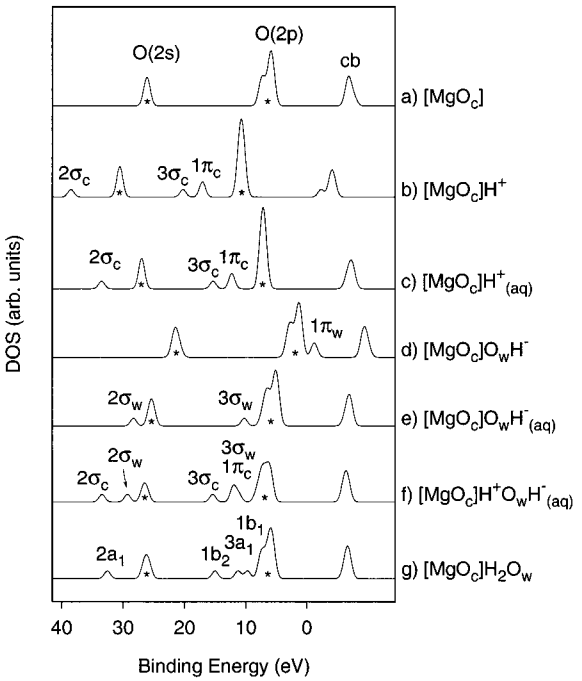

Figure 4. Calculated density of states. The conduction band states are labeled "cb", and an asterisk is used to mark the position of O(2s) and O(2p) crystal bands. "c" and "w" notations indicate features due to the O_cH^- and O_wH^- hydroxyls, respectively.

Electronic Density of States. In Figure 4 we present the calculated densities of states for some adsorbate configurations considered in this work. As suggested earlier,[35] to attain the best agreement between calculated DOS and experimental MIES spectra for MgO, our density of states graphs were generated by smoothing of calculated orbital energy levels with Gaussian functions having a width of 1.0 eV at half-maximum. Useful insight from the DOS features can be drawn from the relative positions of bands rather than from the absolute binding energies of the particular features. This is true because orbital energies resulting from HF calculations are referenced to vacuum as the zero of energy. However, the experimental zeros of energy in the MIES spectra of Figures 1 and 2 are at the Fermi level of molybdenum, which has been used as a substrate for growing MgO films in those experiments. Therefore, to facilitate comparison of our calculated DOS with experiment, the binding energy scale of Figure 4 was shifted by an amount equal to the work function of molybdenum (4.5 eV). This adjustment places our calculated DOS on approximately the same energy scale as the MIES spectra. In Table 2 we list the relative positions of the DOS features with reference to the top of the valence band. Theoretical positions were determined by defining the highest eigenvalue in the O(2p) band as the valence band edge. Energy differences were then taken between this reference point and the levels of interest. Shown in parentheses in Table 2 are the experimental positions of DOS features relative to the O(2p) band edge at 3.8 eV according to the MIES spectra presented in Figures 1a and 2a.

TABLE 2: Positions of DOS Features (eV) with Respect to the Top of the Valence Band (experimental numbers in parentheses)

feature	Figure 4b O_cH^-(g)	Figure 4c O_cH^- (aq)	Figure 4d O_wH^-(g)	Figure 4e O_wH^-(aq)	Figure 4f O_wH^-(aq) O_cH^-(aq)	Figure 4g H_2O
$1b_1$						4.3 (3.4)
$3a_1$						5.8 (5.4)
$1b_2$						9.6 (9.8)
$1\pi_w(d_2)$			−2.2	2.4	1.5 (1.6)	
$3\sigma_w(d_1)$			2.2	5.5	5.3 (6.1)	
$1\pi_c$	6.8	5.5			6.2	
$3\sigma_c$	10.0	8.6			9.5	

Figure 4a shows the DOS for the clean MgO(100) surface and provides a baseline for comparison to other adsorption complexes. Upon adsorption of H^+ (see Figure 4b), the entire spectrum shifts to higher electron binding energies relative to the MgO(100) surface. As was explained in refs 14, 56, and 57, this shift is due to the positive electrostatic potential generated in the cluster by the presence of a proton. The local electronic structure of the proton adsorbed on the crystal oxygen (O_c) is similar to that in an OH^- ion. This adsorption complex gives a $2\sigma_c$ peak below the oxygen 2s valence band and a double-peak structure below the O(2p) valence band.[14,58] The latter peaks are labeled as $3\sigma_c$ and $1\pi_c$ according to the molecular orbital classification in OH^-. In the presence of water, polarization induces a negative potential in the vicinity of the H^+ adsorption site; this reduces the splitting of H^+-induced features from the crystal bands (see Figure 4c).

In agreement with other calculations,[14,58] adsorption of OH^- produces a structure in the band gap region near the top of the O(2p) valence band (labeled $1\pi_w$ in Figure 4d). The $2\sigma_w$ and $3\sigma_w$ features are hidden inside the valence bands. In the presence of water (Figure 4e), polarization induces a positive potential around OH^-, so adsorption-induced levels shift to higher binding energies and $2\sigma_w$ and $3\sigma_w$ levels appear below the oxygen 2s and 2p valence bands, respectively. In this case the $1\pi_w$ peak is inside the oxygen 2p valence band.

The DOS for water dissociated at the MgO−water interface (Figure 4f) exhibits features of both adsorbed H^+ and OH^-. All peaks, except for $1\pi_w$, are well-separated from crystal bands, and the $3\sigma_w$ and $1\pi_c$ peaks overlap. In an attempt to understand how much the dielectric solvent contributes to the DOS of dissociated water, we performed a calculation for total energy of dissociatively adsorbed water at the fixed geometry shown in Figure 3, this time with the solvent removed. As explained above, this structure does not correspond to a stable minimum at the solid−vacuum interface. Thus, if this geometry were allowed to relax, the system would step toward the structure characteristic for molecularly adsorbed water. The resulting DOS was virtually the same as with the solvent present (Figure 4f) in regard to the features observable by MIES. This result indicates that a solvent is important for stabilizing the hydroxyl pair but does not significantly change the electronic structure of dissociated water at the MgO(100)−water interface.

Adsorption of molecular water induces levels (labeled $1b_1$, $3a_1$, and $1b_2$ in Figure 4g) that split to higher binding energies from the O(2p) core peak. This DOS structure is very similar with and without the dielectric present;[26] however, perturbations of these water features occur in relation to the presence of the surface. In comparison to a free water molecule in vacuum, adsorption stabilizes the $1b_1$ orbital due to its having electron density directed toward Mg^{2+}. As shown in Table 2, we have good agreement between the positions of water-induced peaks ($1b_1$, $3a_1$, and $1b_2$) from the MIES spectra and our theoretical predictions.

4. Discussion

Since no formation of surface hydroxyls could be observed in the MIES data of Figure 1, the adsorption of water on the MgO(100) surface at 100 K appears to be nondissociative. In a recent MIES experiment,[28] we have shown that we are able to detect the formation of surface hydroxyls during the adsorption of Na on a water multilayer at 100 K with a high sensitivity. Thus, due to the high surface sensitivity of MIES, especially the dissociation of water at the water−vacuum interface can be excluded. As shown in a recent study by Heidberg et al.,[5] it is possible to prepare a monolayer water on MgO(100) by dosing water at 152 K substrate temperature; in agreement with other studies, e.g., ref 2, no dissociation products have been observed. This is also consistent with previous theoretical studies and our own calculations performed on the clean MgO surface. Therefore, we can also exclude the formation of surface hydroxyls on the defect-free MgO(100) surface in the monolayer coverage regime.

However, after dosing the MgO surface to multilayer coverage and annealing the water-covered MgO surface to 155 K, the appearance of hydroxyl-induced features (d_1 and d_2 in Figure 2) indicates a partial dissociation of water molecules. A possible explanation for the appearance of hydroxyl features in the MIES spectra of Figure 2 is given by our theoretical results presented in section 3. While water dissociation at the MgO(100)−vacuum interface is not energetically favorable, polarization of the surrounding medium stabilizes charged dissociation products at the MgO(100)−water interface. Therefore, water dissociation at this interface after multilayer water adsorption could be one explanation for the hydroxyl features in the MIES spectra.

Molecular dynamics simulations indicate the absence of significant structure in the liquid phase beyond the first two monolayers of water adsorbed on MgO.[27] Therefore, multilayer water coverage (about 3 ML), as in the MIES experiments, is believed to be sufficient to create a condition near the MgO crystal surface that is very similar to the MgO−water interface environment. In this multilayer coverage regime, our results indicate that water molecules dissociate at the interface; however, the hydroxyl products of such a dissociation are not seen in our spectra due to the surface sensitivity of MIES. Rather, water molecules at the top of the multilayer are visible. Upon raising the temperature, molecular water desorbs and hydroxyls become exposed at about 155 K. Indeed, hydroxyl features are visible in the MIES spectra up to 400 K, well above the temperature that water is desorbed from the surface (see TPD spectrum of Figure 2a). Our calculations show that a solvent is necessary to stabilize the ion pair, which upon removal of the solvent should recombine, but such a recombination after the loss of molecular water is not obvious in the MIES data. It is difficult to say how many water molecules around the OH^-−H^+ pair are sufficient to prevent recombination and desorption into the gas phase. A layer of adsorbed molecular water (at 1 ML coverage) or a cluster of just a few water molecules (at submonolayer coverage) around the OH^-−H^+ pair could be sufficient to preserve these species following their formation. In this case, features from both adsorbed O_wH^- and molecular H_2O would be visible in MIES spectra. However, we would expect the H_2O-induced peaks to be weaker than O_wH^- peaks because O_wH^- species are protruding above the layer of adsorbed water molecules laying essentially flat on the surface.[26,27,59] Since the balance between solvation and reaction of dissociation products at the water−substrate interface is an important factor, the surface chemistry which may occur in an aqueous environment is relatively complicated. Taking this into

consideration, it is unclear which role the surface topography, i.e., the existence of point and extended defects like steps and kinks, plays in the stabilization of dissociation products after the complete desorption of water at elevated temperatures.

We have also recorded temperature-dependent MIES measurements taken from the MgO(100) surface covered by water in a coverage regime below 0.5 ML, in order to avoid 3D growth. In those experiments a formation of surface hydroxyls after the desorption of water at temperatures over 195 K was also noticeable; however, their intensity in MIES was very small, and no prominent hydroxyl feature together with intensity from the ionization of water, comparable to the 155 K spectrum in Figure 2, could be observed. In this context, the appearance of a small number of surface hydroxyls after annealing the MgO surface precovered by water in a submonolayer coverage regime can be explained by the existence of reactive surface sites, such as surface defects, as well. On the other hand, as suggested in ref 60, we have to take into consideration a possible dissociation of the water molecules on the defect-free MgO(100) surface in the recently observed (3×2) water overlayer. However, the fact that no formation of surface hydroxyls could be observed in Figure 1 during the water adsorption at 100 K, even at very low coverages, suggests that the water dissociation needs to be thermally activated.

Aside from what has been discussed above, there are other possibilities for the appearance of hydroxyl features in the MIES spectrum. In the presence of multilayer water the surface may reconstruct or begin dissolution. Thus, formation of species such as $MgOH^+$ and $Mg(OH)_2$ is possible.[17] These species may remain on the surface even after desorption of multilayer water and give rise to hydroxyl levels in the MIES spectrum.

The appearance of hydroxyl features raises questions with regard to the nature of such hydroxyl groups that may exist on this MgO surface. We can address these questions with results from our theoretical study. There are essentially three types of hydroxyls to consider: (i) a protonated surface oxygen ion; (ii) an adsorbed hydroxyl group; (iii) both (i) and (ii) in close proximity and in the presence of a solvent as in Figure 3. The calculated DOS of a type (i) hydroxyl group (Figure 4b,c) is distinguished by a doublet that is significantly displaced to higher binding energies from the oxygen 2p band. This is not consistent with the d_1 and d_2 features of the MIES spectra. A type (ii) hydroxyl group at the MgO−vacuum interface is characterized by a level in the band gap (Figure 4d), and the MIES spectra show no such levels. However, the positions of the hydroxyl peaks ($3\sigma_w$ and $1\pi_w$) in a type (iii) hydroxyl complex (Table 2 and Figure 4f) are in good agreement with the MIES spectra of Figure 2. Therefore, we have assigned the d_1 feature of the MIES spectra to the $3\sigma_w$ hydroxyl level and the d_2 feature to $1\pi_w$. Recall from our DOS presentation in section 3.2 that $1\pi_w$ is obscured by the oxygen 2p crystal band and therefore has not been labeled in Figure 4f.

We are less certain about the assignment of $3\sigma_c$ and $1\pi_c$ peaks. Due to its energetic position, the $1\pi_c$ level may contribute to the d_1 feature; also one can interpret the slight shift of the $1b_2$ peak in Figure 2 to higher binding energies with increasing temperature as a formation of the $3\sigma_c$ peak. However, the assignments of these crystal hydroxyl levels are rather speculative at this point because the location at which one would expect to find the $3\sigma_c$ level in a MIES spectrum is close to the steep increase of the intensity originating from secondary electrons and is near the cutoff of the spectrum. Moreover, even if $3\sigma_c$ and $1\pi_c$ features are present in Figure 2, they may be rather weak because the O_cH hydroxyls could be shielded by O_wH-type hydroxyl groups and are perhaps not fully visible using the surface-sensitive MIES technique. Safely, we have detected only one class of OH species with MIES on the surface after desorption of multilayer water.

The result that hydroxylation of the MgO(100)−water interface lowers its energy offers a natural explanation for periclase transformation to brucite and dissolution of MgO in water. Low-coordinated surface sites and high-index surface planes need not be involved. The point should also be made that water dissociates not because the aqueous solvent increases the reactivity of the MgO surface. It has been established in other studies that higher ionicity of low-coordinated surface sites on MgO usually implies their lower reactivity (for more details see ref 24 and references therein). It was reported in article 1 that hydration of the MgO(100) surface, as modeled by CECILIA, increases the surface ionicity. Therefore, we expect a hydrated surface alone to be less reactive than the clean surface. In practice, however, it is polarization of the surrounding solvent that is responsible for stabilization of charged dissociation products. This result is similar to that found in the case of the NaCl−water interface,[22] where solvent effects were found to be more significant in regard to interfacial reactivity than interactions with the ionic crystal surface. It is difficult to judge from our cluster calculations whether a fully hydroxylated MgO(100)−water interface is energetically stable. Answering such a question requires studies on coverage dependence of the interactions in the hydroxyl layer. This is beyond the capabilities of the cluster model used in our present investigation.

5. Conclusions

Using the surface-sensitive technique of MIES, we have identified the presence of two new features in the spectrum after multilayer water desorption from MgO(100). These new features resemble a hydroxyl doublet that could result from the dissociation of water at the interface of MgO(100) and multilayer water. Our theoretical results suggest that dissociative adsorption of water becomes favorable at the MgO(100)−water interface. This result can only be obtained if solvent effects are properly taken into account. On the basis of the relative positions of calculated DOS peaks, we have assigned the new features in the MIES spectra to the $3\sigma_w$ and $1\pi_w$ hydroxyl levels that result when a water molecule dissociatively chemisorbs at the MgO(100)−water interface. Our calculations predict that protonated surface oxygen anions coexist with adsorbed hydroxide ions and may also contribute to the MIES spectra, giving $3\sigma_c$ and $1\pi_c$ features, but these are not clearly evident using MIES.

The result that charged species at the MgO−water interface are stabilized by polarization of the water phase should be applicable to a wide variety of adsorption processes at solid−liquid interfaces providing the liquid phase is composed of a polar solvent.

Acknowledgment. T.N.T. wishes to acknowledge support from the National Science Foundation through a Young Investigator Award. D.W.G. acknowledges with pleasure the support of this work by the National Science Foundation (Contract No. DMR 9423707) and the Laboratory Directed Research and Development (LDRD) funding from Pacific Northwest Laboratory. Pacific Northwest Laboratory is operated for the U.S. Department of Energy by Battelle Memorial Institute under Contract No. DE-AC06-76RLO 1830.

References and Notes

(1) Boehm, H.-P.; Knözinger, H. *Catalysis: Science and Technology*; Springer-Verlag: Berlin, Heidelberg, New York, 1983; Vol. 4, p 39.

(2) Ferry, D.; Glebov, A.; Senz, V.; Suzanne, J.; Toennies, J. P.; Weiss, H. *J. Chem. Phys.* **1996**, *105*, 1697.
(3) Stirniman, M. J.; Huang, C.; Smith, R. S.; Joyce, S. A.; Kay, B. D. *J. Chem. Phys.* **1996**, *105*, 1295.
(4) Xu, C.; Goodman, D. W. *Chem. Phys. Lett.* **1997**, *265*, 341.
(5) Heidberg, J.; Redlich, B.; Wetter, D. *Ber. Bunsenges. Phys. Chem.* **1995**, *99*, 1333.
(6) Scamehorn, C. A.; Hess, A. C.; McCarthy, M. I. *J. Chem. Phys.* **1993**, *99*, 2786.
(7) Chacon-Taylor, M. R.; McCarthy, M. I. *J. Phys. Chem.* **1996**, *100*, 7610.
(8) de Leeuw, N. H.; Watson, G. W.; Parker, S. C. *J. Phys. Chem.* **1995**, *99*, 17219.
(9) Tikhomirov, V. A.; Geudtner, G.; Jug, K. *J. Phys. Chem. B* **1997**, *101*, 10398.
(10) Kuroda, Y.; Yasugi, E.; Aoi, H.; Miura, K.; Morimoto, T. *J. Chem. Soc., Faraday Trans. 1* **1988**, *84*, 2421.
(11) Coluccia, S.; Marchese, L.; Lavagnino, S.; Anpo, M. *Spectrochim. Acta* **1987**, *43A*, 1573.
(12) Onishi, H.; Egawa, C.; Aruga, T.; Iwasawa, Y. *Surf. Sci.* **1987**, *191*, 479.
(13) Almeida, A. L.; Martins, J. B. L.; Taft, C. A.; Longo, E.; Lester, W. A., Jr. *J. Chem. Phys.* **1998**, *109*, 3671.
(14) Goniakowski, J.; Noguera, C. *Surf. Sci.* **1995**, *330*, 337.
(15) Scamehorn, C. A.; Harrison, N. M.; McCarthy, M. I. *J. Chem. Phys.* **1994**, *101*, 1547.
(16) Refson, K.; Wogelius, R. A.; Fraser, D. G.; Payne, M. C.; Lee, M. H.; Milman, V. *Phys. Rev. B* **1995**, *52*, 10823.
(17) Segall, R. L.; Smart, R. S. C.; Turner, P. S. *Surface and Near-Surface Chemistry of Oxide Materials*; Elsevier Science Publishers B.V.: Amsterdam, 1988; Chapter 13.
(18) Komiyama, M.; Gu, M. *Appl. Surf. Sci.* **1997**, *120*, 125.
(19) Blesa, M. A.; Morando, P. J.; Regazzoni, A. E. *Chemical Dissolution of Metal Oxides*; CRC Press: Boca Raton, FL, 1994.
(20) Zhou, X. L.; Cowin, J. P. *J. Phys. Chem.* **1996**, *100*, 1055.
(21) Ochs, D.; Brause, M.; Stracke, P.; Krischok, S.; Wiegershaus, F.; Maus-Friedrichs, W.; Kempter, V.; Puchin, V. E.; Shluger, A. L. *Surf. Sci.* **1997**, *383*, 162.
(22) Stefanovich, E. V.; Truong, T. N. *J. Chem. Phys.* **1997**, *106*, 7700.
(23) Stefanovich, E. V.; Truong, T. N. *Combined Quantum Mechanical and Molecular Mechanical Methods*; ACS Symposium Series 712: Washington, DC, 1998; Chapter 6.
(24) Stefanovich, E. V.; Truong, T. N. *J. Chem. Phys.* **1995**, *102*, 5071.
(25) Johnson, M. A.; Stefanovich, E. V.; Truong, T. N. *J. Phys. Chem. B* **1997**, *101*, 3196.
(26) Johnson, M. A.; Stefanovich, E. V.; Truong, T. N. *J. Phys. Chem. B* **1998**, *102*, 6391; to be referred to as article 1.
(27) McCarthy, M. I.; Schenter, G. K.; Scamehorn, C. A.; Nicholas, J. B. *J. Phys. Chem.* **1996**, *100*, 16989.
(28) Günster, J.; Liu, G.; Kempter, V.; Goodman, D. W. *J. Vac. Sci. Technol. A* **1998**, *16*, 996.
(29) Harada, Y.; Masuda, S.; Ozaki, H. *Chem. Rev.* **1997**, *97*, 1897.
(30) Maus-Friedrichs, W.; Wehrhahn, M.; Dieckhoff, S.; Kempter, V. *Surf. Sci.* **1990**, *237*, 257.
(31) Maus-Friedrichs, W.; Dieckhoff, S.; Kempter, V. *Surf. Sci.* **1991**, *249*, 149.
(32) Wu, M. C.; Corneille, J. S.; Estrada, C. A.; He, J. W.; Goodman, D. W. *Chem. Phys. Lett.* **1991**, *182*, 472.
(33) Wu, M. C.; Truong, C. M.; Goodman, D. W. *Phys. Rev. B* **1992**, *46*, 12688.
(34) Ferry, D.; Glebov, A.; Senz, V.; Suzanne, J.; Toennies, J. P.; Weiss, H. *Surf. Sci.* **1997**, *377*−*379*, 634.
(35) Ochs, D.; Maus-Friedrichs, W.; Brause, M.; Günster, J.; Kempter, V.; Puchin, V.; Shluger, A.; Kantorovich, L. *Surf. Sci.* **1996**, *365*, 557.
(36) Tjeng, L. H.; Vos, A. R.; Sawatzky, G. A. *Surf. Sci.* **1990**, *235*, 269.
(37) Turner, D. W.; Baker, C.; Baker, A. D.; Brundle, C. R. *Molecular Photoelectron Spectroscopy*; Wiley: New York, 1970.
(38) Banna, M. S.; McQuaide, B. H.; Malutzki, R.; Schmidt, V. *J. Chem. Phys.* **1986**, *84*, 4739.
(39) Čermák, V.; Yencha, A. J. *J. Electron Spectrosc. Relat. Phenom.* **1977**, *11*, 67.
(40) Günster, J.; Stultz, J.; Liu, G.; Krischok, S.; Goodman, D. W. Manuscript in preparation.
(41) Thiel, P. A.; Madey, T. E. *Surf. Sci. Rep.* **1987**, *7*, 211.
(42) Truong, T. N.; Stefanovich, E. V. *J. Chem. Phys.* **1995**, *109*, 3709.
(43) Anchell, J. L.; Hess, A. C. *J. Phys. Chem.* **1996**, *100*, 18317.
(44) Stevens, W. J.; Basch, H.; Krauss, M. *J. Chem. Phys.* **1984**, *81*, 6026.
(45) Stefanovich, E. V.; Truong, T. N. *J. Chem. Phys.* **1996**, *105*, 2961.
(46) Truong, T. N.; Stefanovich, E. V. *J. Phys. Chem.* **1995**, *99*, 14700.
(47) Truong, T. N.; Nguyen, U. N.; Stefanovich, E. V. *Int. J. Quant. Chem.*: *Quant. Chem. Symp.* **1996**, *30*, 403.
(48) Truong, T. N.; Truong, T.-T. T.; Stefanovich, E. V. *J. Chem. Phys.* **1997**, *107*, 1881.
(49) Truong, T. N.; Stefanovich, E. V. *Chem. Phys. Lett.* **1995**, *240*, 253.
(50) Stefanovich, E. V.; Truong, T. N. *Chem. Phys. Lett.* **1995**, *244*, 65.
(51) Pascual-Ahuir, J. L.; Silla, E.; Tuñón, I. *J. Comput. Chem.* **1994**, *15*, 1127.
(52) Weast, R. C., Astle, M. J., Eds. *CRC Handbook of Chemistry and Physics*, 62nd ed.; CRC Press: Boca Raton, FL, 1981−1982.
(53) Pacchioni, G.; Ferrari, A. M.; Márquez, A. M.; Illas, F. *J. Comput. Chem.* **1997**, *18*, 617.
(54) Tuñón, I.; Silla, E.; Bertrán, J. *J. Phys. Chem.* **1993**, *97*, 5547.
(55) Reiss, H.; Heller, A. *J. Phys. Chem.* **1985**, *89*, 4207.
(56) Russo, S.; Noguera, C. *Surf. Sci.* **1992**, *262*, 245.
(57) Russo, S.; Noguera, C. *Surf. Sci.* **1992**, *262*, 259.
(58) Goniakowski, J.; Bouette-Russo, S.; Noguera, C. *Surf. Sci.* **1993**, *284*, 315.
(59) Marmier, A.; Hoang, P. N. M.; Picaud, S.; Girardet, C.; Lynden-Bell, R. M. *J. Chem. Phys.* **1998**, *109*, 3245.
(60) Giordano, L.; Goniakowski, J.; Suzanne, J. *Phys. Rev. Lett.* **1998**, *81*, 1271.